O. A Survey of Critical Experiments

(A) Visualizations of Turbulent Flow

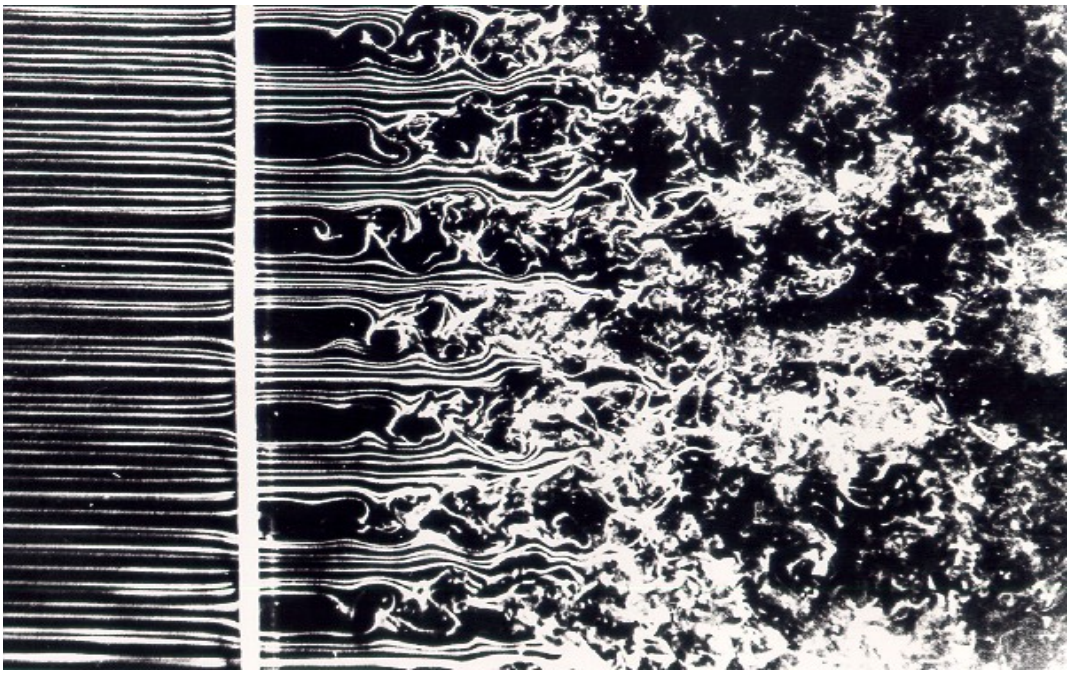

Figure 1: Van Dyke, Album of Fluid Motion #152. Generation of turbulence by a grid. Smoke wires show a uniform laminar stream passing through a 1/16-inch plate with 3/4-inch square perforations. The Reynolds number is 1500 based on the 1-inch mesh size. Instability of the shear layers leads to turbulent flow downstream. Photograph by Thomas Corke and Hassan Nagib.

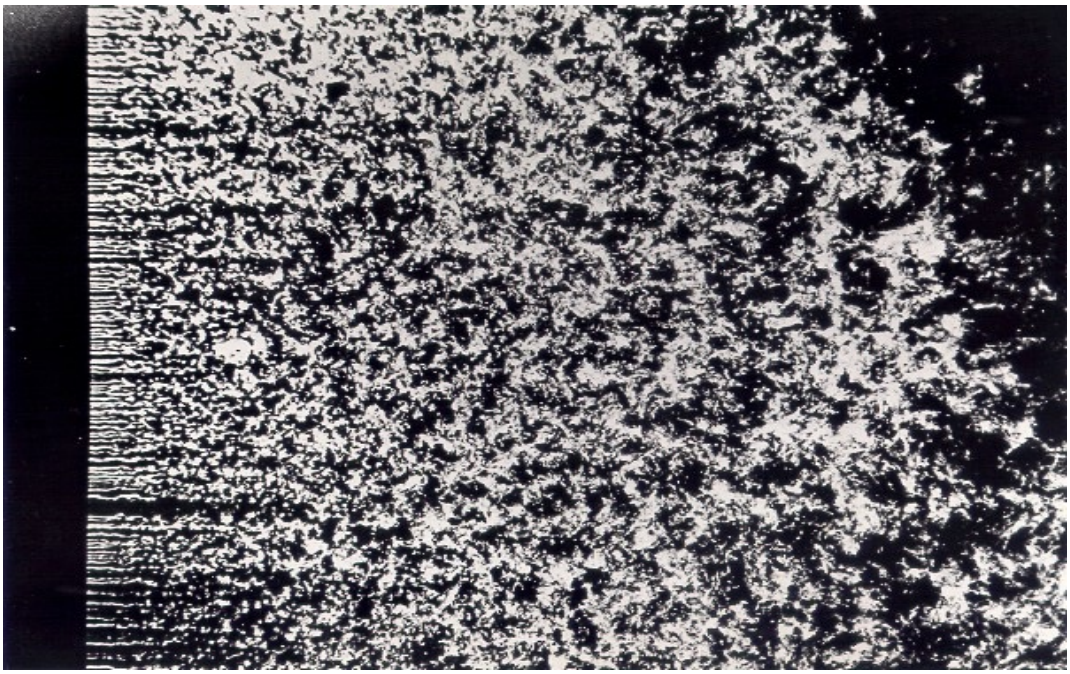

Figure 2: Van Dyke, Album of Fluid Motion #153. Homogeneous turbulence behind a grid. Behind a finer grid than above, the merging unstable wakes quickly form a homogeneous field. As it decays downstream, it provides a useful approximation to the idealization of isotropic turbulence. Photograph by Thomas Corke and Hassan Nagib.

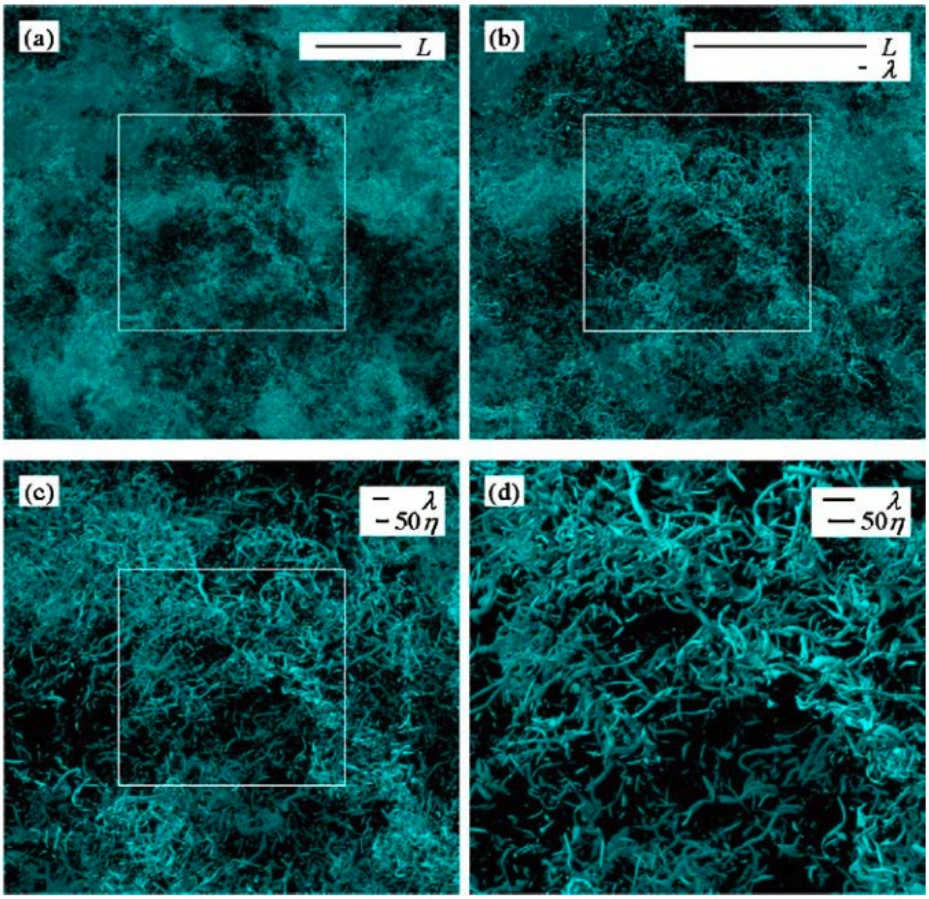

Figure 3. Intense-vorticity isosurfaces showing the region where $\omega > \langle\omega\rangle + 4\sigma_\omega$. $R_\lambda = 732$. (a) The size of the display domain is $(5984^2 \times 1496)\,\eta^3$, periodic in the vertical and horizontal directions. (b) Close-up view of the central region of (a) bounded by the white rectangular line; the size of display domain is $(2992^2 \times 1496)\,\eta^3$. (c) Close-up view of the central region of (b); $1496^3\eta^3$ (d) Close-up view of the central region of (c); $(748^2 \times 1496)\,\eta^3$.

Figure 3: From Y. Kaneda and T. Ishihara, High-resolution direct numerical simulation of turbulence, Journal of Turbulence, Volume7, No.20, 2006

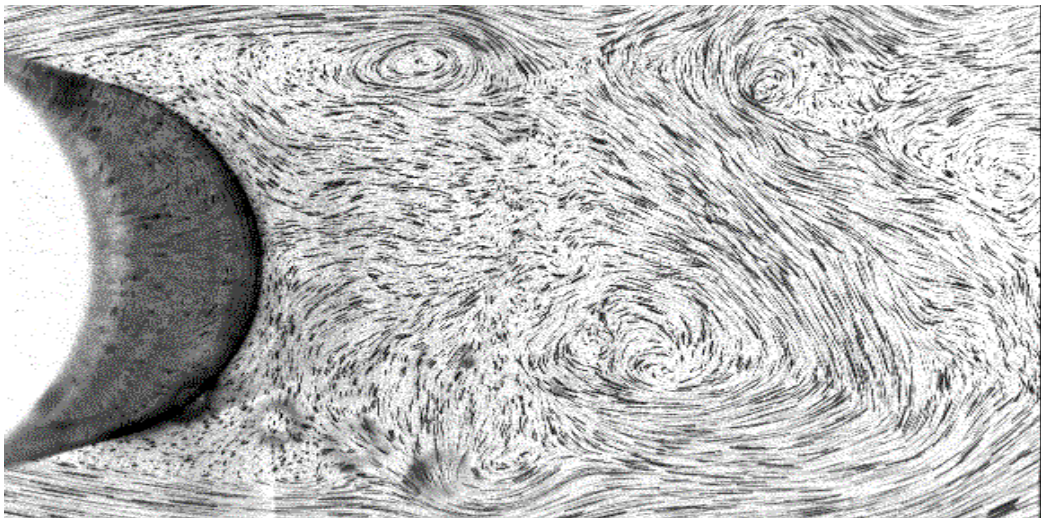

Figure 4: From http://www.eng.fsu.edu/ shih/succeed/cylinder/flow%20vis/shedding.gif.

Turbulent wake flow behind a circular cylinder, visualized by Particle Imaging Velocimetry (PIV).

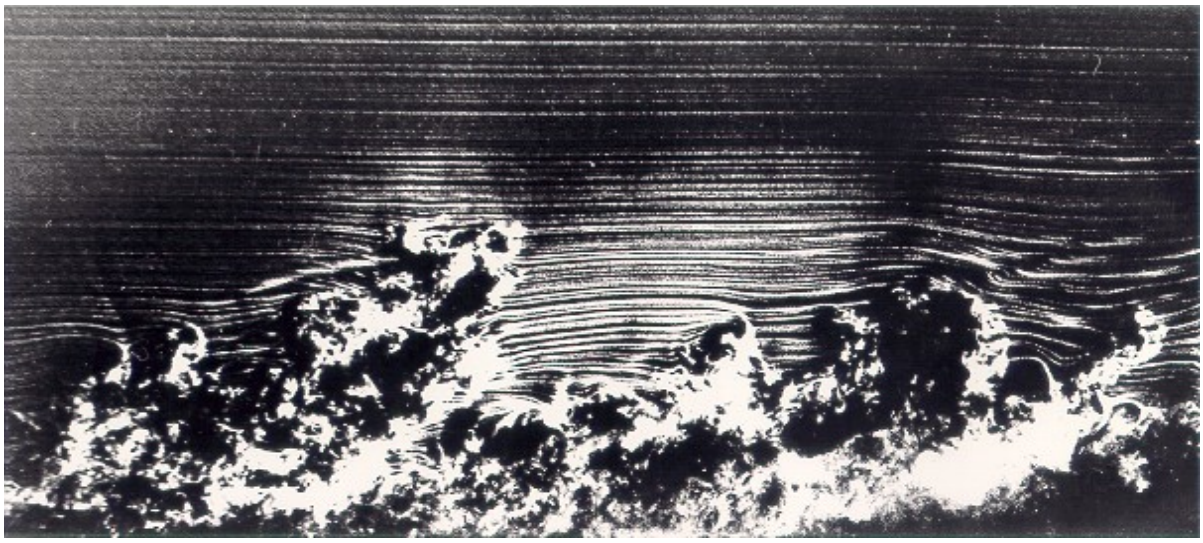

Figure 5: Van Dyke, Album of Fluid Motion #157. Sideview of a turbulent boundary layer. Here a turbulent boundary layer develops naturally on a flat plate 3.3m long suspended in a wind tunnel. Streaklines from a smoke wire near the sharp leading edge are illuminated by a vertical slice of light. The Reynolds number is 3500 based on the momentum thickness. The intermittent nature of the outer part of the layer is evident. Photograph by Thomas Corke, Y. Guezennec and Hassan Nagib.

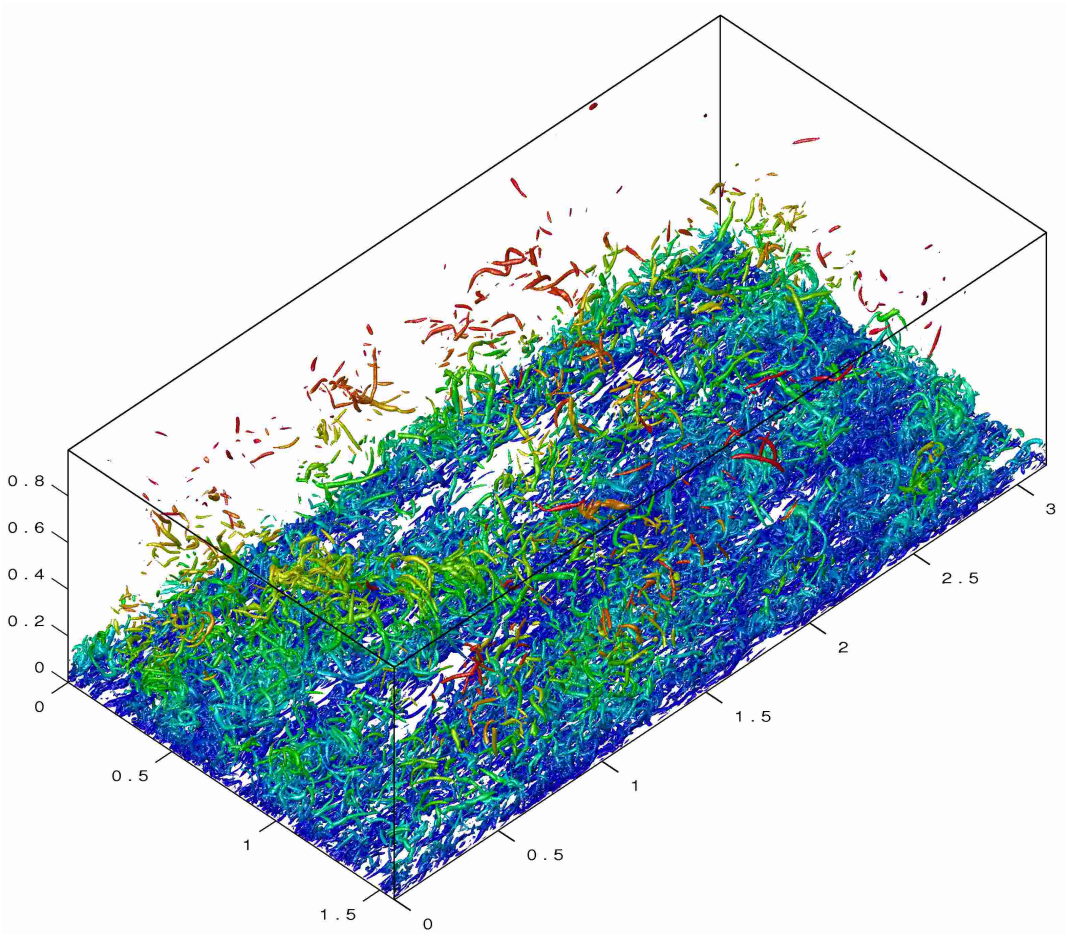

Figure 6: From http://torroja.dmt.upm.es/ftp/channels. Isosurface of the discriminant of the velocity gradient tensor for an instantaneous realization of a $Re_\tau = 1900$ turbulent channel (J.C. del Alamo, J. Jimenez, P. Zandonade and R.D. Moser 2006, Self-similar vortex clusters in the turbulent logarithmic region. J. Fluid Mech. 561, 329-358)

I Quantitative Estimates of Energy Dissipation Rates

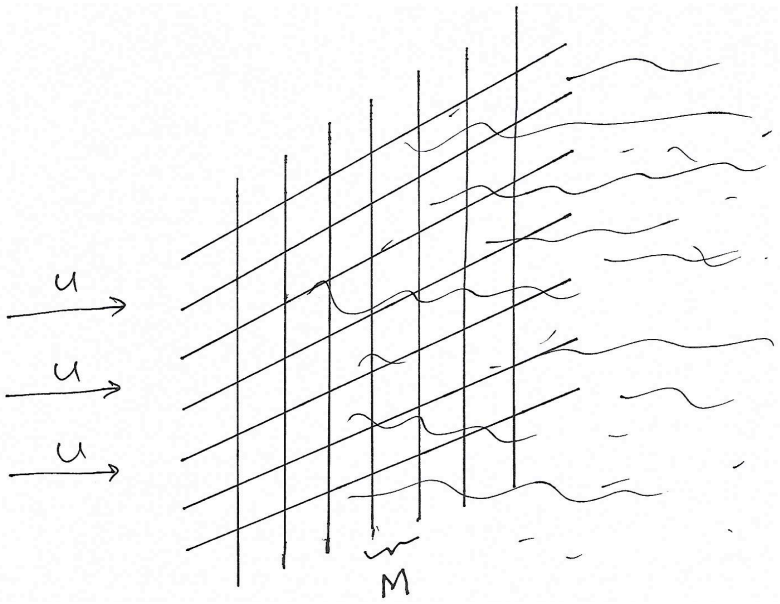

Figure 7: Sketch of grid-generated turbulence.

The rate of decay of kinetic energy (per unit mass) can be measured from

$$\varepsilon \simeq -\frac{D}{Dt}\frac{1}{2}(u')^2 \simeq -U\frac{\partial}{\partial x}\frac{1}{2}(u')^2 \qquad \text{(Taylor hypothesis)}$$

It can be non-dimensionalized by U^3/M or by $(u')^3/L$, where L is the spatial correlation-length or "integral length" of the velocity. The experimental evidence is that

$$\varepsilon \sim C\frac{U^3}{M} \quad \text{or} \quad C'\frac{(u')^3}{L}. \qquad (*)$$

with prefactors C and C' that become independent of $Re_M = UM/\nu$ and $Re_L = u'L/\nu$ when $Re_M \gg 1$, $Re_L \gg 1$.

The fundamental relation (*) was first proposed semi-phenomenologically for pipe-flow data by G. I. Taylor, "Statistical Theory of Turbulence," Proc. Roy. Soc. Lond. A 151: 421 (1935).

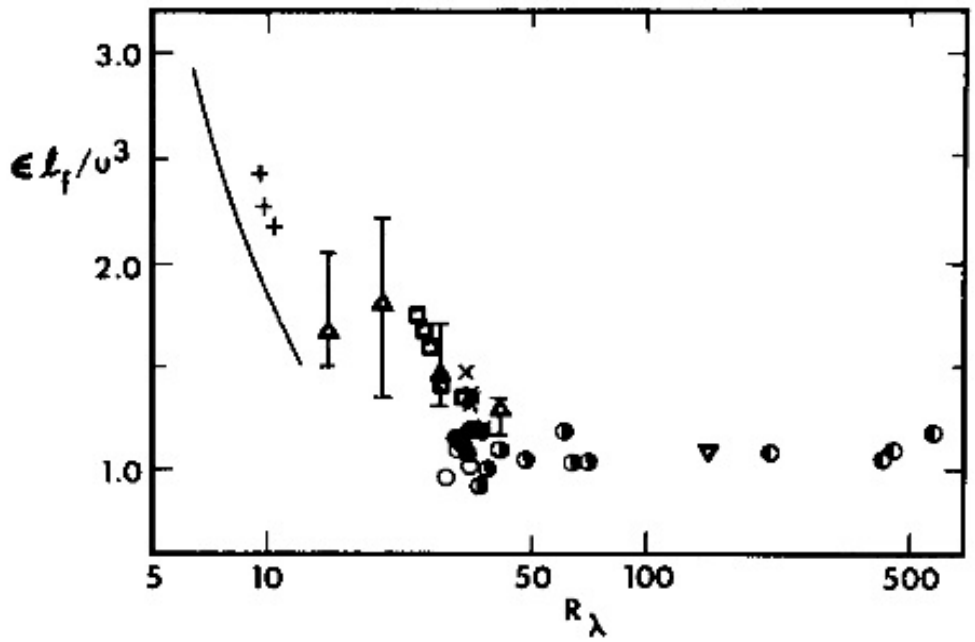

FIG. 1. The quantity $\epsilon L_f/u^3$ for biplane square-mesh grids. All data except + are for the initial period of delay, and are explained in Table I. + indicate typical data[13] in the final period of decay. — corresponds to Eq. (1).

Figure 8: From K. R. Sreenivasan, On the scaling of the turbulence energy dissipation rate, Phys. Fluids 27: 1048-1051 (1984), showing near-independence from $Re = u'L/\nu$.

Phys. Fluids, Vol. 15, No. 2, February 2003

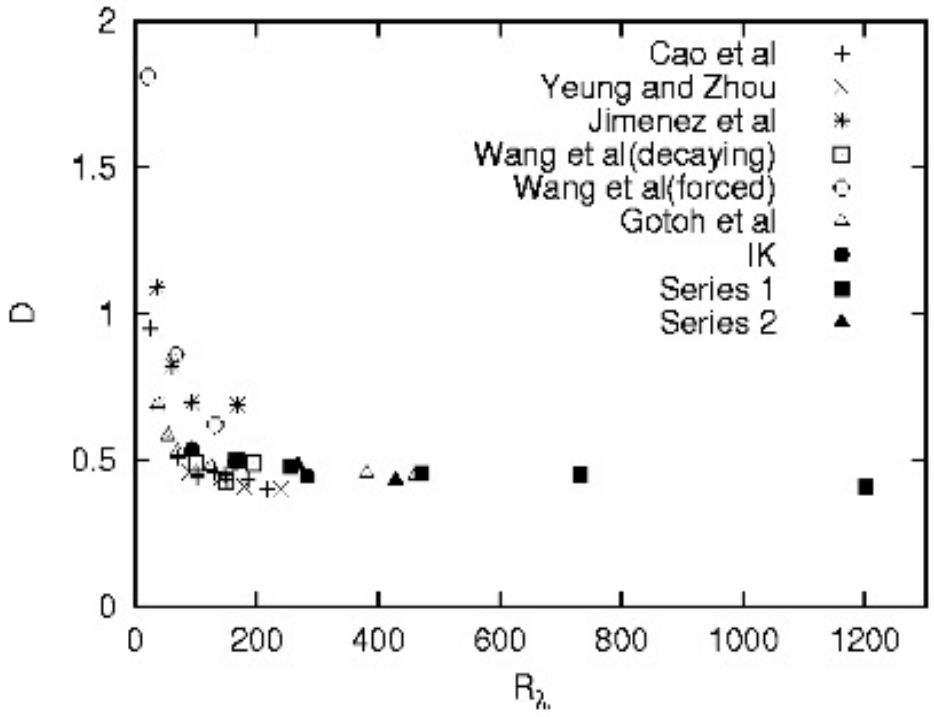

FIG. 3. Normalized energy dissipation rate D versus R_λ from Ref. 5 (data up to $R_\lambda = 250$), Ref. 3 (△,●), and the present DNS databases (■,▲).

Figure 9: From Y. Kaneda et al., Energy dissipation rate and energy spectrum in high resolution direct numerical simulations of turbulence in a periodic box, Phys. Fluids, vol. 15, No. 2, L21-L24 (2003).

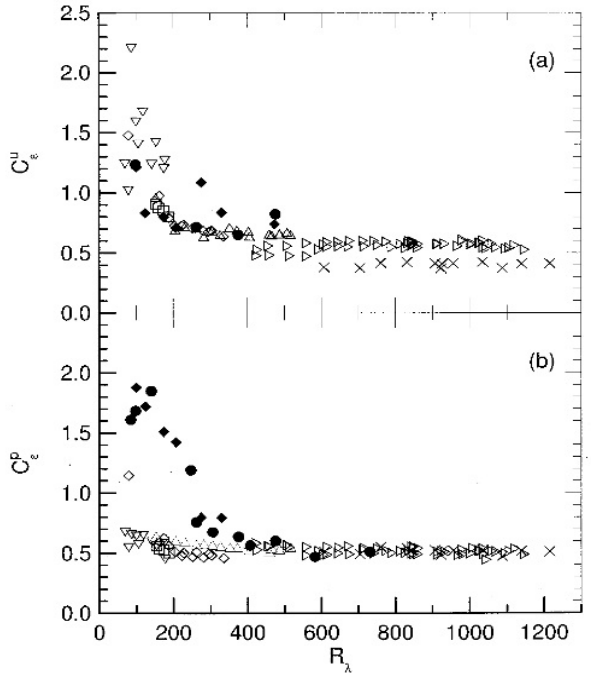

FIG. 1. Normalized dissipation rate for a number of shear flows. Details as found in this work and Refs. 14–16. (a) C_ϵ^u [Eq. (3)]; (b) C_ϵ^p [Eq. (4)]. □, circular disk, $154 \lesssim R_\lambda \lesssim 188$; ▽, pipe, $70 \lesssim R_\lambda \lesssim 178$; ◇, normal plate, $79 \lesssim R_\lambda \lesssim 335$; △, NORMAN grid, $174 \lesssim R_\lambda \lesssim 516$; × NORMAN grid (slight mean shear, $dU/dy \approx dU/dy|_{\max}/2$), $607 \lesssim R_\lambda \lesssim 1217$; ▷, NORMAN grid (zero mean shear), $425 \lesssim R_\lambda \lesssim 1120$; ●, "active" grid Refs. 14, 15, $100 \lesssim R_\lambda \lesssim 731$; ◆, "active" grid, with L_u estimated by Ref. 16. For Ref. 14 data, we estimate $L_p \approx 0.1$ m and for Ref. 15 data we estimate $L_p \approx 0.225$ m.

Figure 10: From B. R. Pearson et al. Measurements of the turbulent energy dissipation rate, Phys. Fluids, vol. 14, No. 3, 1288-1290 (2002). One-dimensional surrogate for the dimensionless energy dissipation rate C is measured in shear flows over a range of the Taylor microscale Reynolds number Re_λ, $70 < Re_\lambda < 1217$.

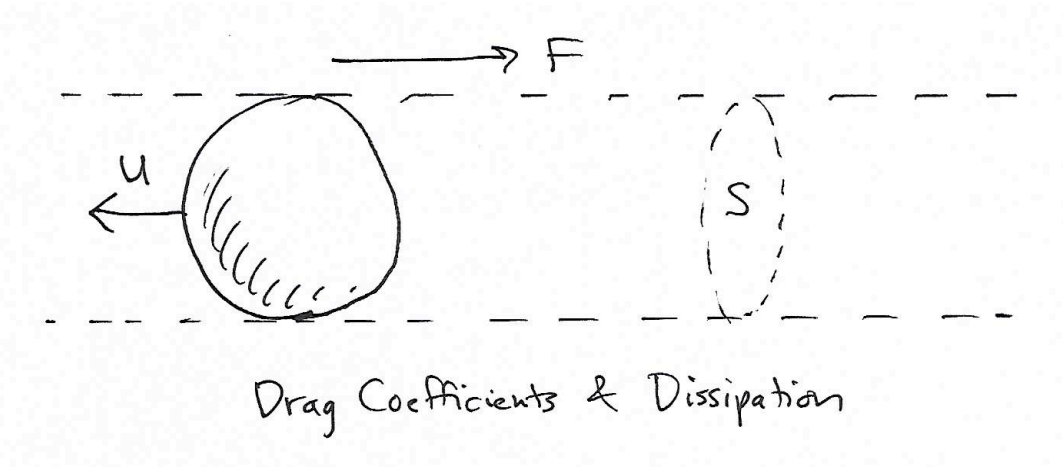

In time $\Delta\tau$, the sphere displaces a volume $V = U\Delta\tau \times S$ of air at rest. If all of its momentum is transferred to the sphere, that implies a change in the momentum of the sphere of $\Delta P = -M \cdot U = -\rho V \cdot U$, or

$$\Delta P = -\rho S U^2 \Delta\tau.$$

and thus a force $F = \Delta P/\Delta\tau$, or

$$F = -\rho S U^2.$$

In fact, only a fraction of the momentum of the air, conventionally denoted $\frac{1}{2}C_D$, is transferred, leading to a formula for the drag force

$$F = -\frac{1}{2} C_D \rho S U^2,$$

where C_D is the drag coefficient.

By hydrodynamic similarity, we may rescale lengths by $L = \sqrt{S}$, velocities by U, times by $T = L/U$, and masses by $M = \rho L^3$. Since

$$[F] = (mass)\frac{length}{time^2} = density \times length^2 \times velocity^2$$

it follows that

$$F = -\frac{1}{2}C_D(Re)\rho S U^2,$$

where C_D is a function only of the Reynolds number $Re = \frac{UL}{\nu}$.

Experimental evidence seems to indicate that

$$\lim_{re\to\infty} C_D(Re) = C_D(\infty) > 0.$$

For example, see Figure 34 in Landau & Lifschitz, Fluid Mechanics, 2nd Edition (1987). There is a little "glitch" around $Re \doteq 2 - 3 \times 10^5$, called the drag crisis. But thereafter it appears that $C_D(Re)$ asymptotes to a nonzero limit.

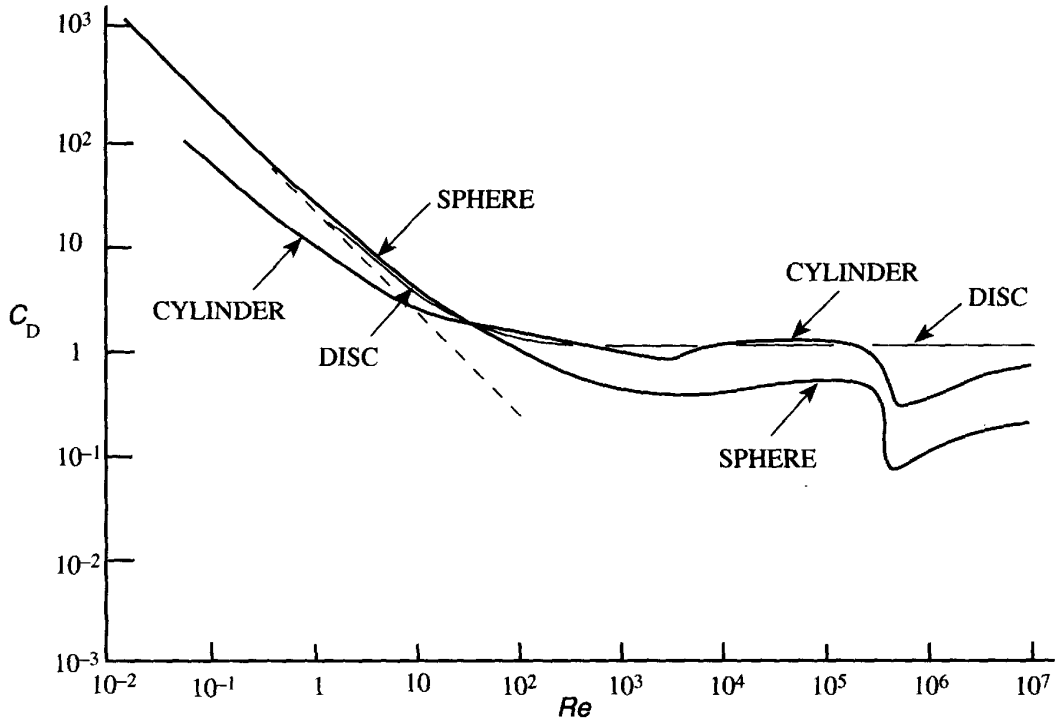

Figure 7.13 Log–log plot of drag coefficient C_D as a function of Reynolds Number *Re* for spheres, transverse cylinders, and face-on discs. The broken straight line represents Stokes's law.

Figure 11: From http://misclab.umeoce.maine.edu/boss/boss.php

The power input to move the sphere is

$$\mathcal{P} = FU = \frac{1}{2} C_D(Re) \rho L^2 U^3.$$

This power input is dissipated by heating in the turbulent wake of the object, which has a volume $\sim L^3$ (again by hydrodynamic similarity). Thus, the energy dissipation in the turbulence per unit mass, ε, is given by

$$\begin{aligned} \varepsilon = \frac{\mathcal{P}}{M} &\sim \frac{\frac{1}{2} C_D(Re) \rho L^2 U^3}{\rho L^3} \\ &= \frac{1}{2} C_D \frac{U^3}{L}. \end{aligned}$$

Thus, as $Re \to \infty$, it appears that

$$\boxed{\varepsilon \sim \frac{U^3}{L}}$$

and is entirely independent of the molecular viscosity ν! This is a fundamental experimental fact about 3D turbulent flow, sometimes called the "zeroth law of turbulence."

Comment: One may define the circulation time L/U to be the time required for a parcel of fluid to move distance L, and the damping time $\frac{1}{2}U^2 \big/ \frac{d}{dt}\left(\frac{1}{2}U^2\right)$ that required for a finite fraction of the energy to be dissipated. Then (*) implies that

$$\begin{aligned} \text{damping time} &= \frac{1}{2}U^2 \Big/ \frac{d}{dt}\left(\frac{1}{2}U^2\right) \\ &= \frac{1}{2}U^2 \Big/ \frac{U^3}{L} \\ &\sim L/U \quad = \text{circulation time} \end{aligned}$$

The turbulence is thus critically damped in some sense, because the circulation or eddy-turnover time is approximately equal to the damping time.

Wall-Bounded Flows

In wall-bounded flows, the situation is somewhat different:

(a) With smooth walls, the dissipation appears to weakly vanish, e.g. $\sim 1/\log Re$, as $Re \to \infty$ (but possibly with a plateau at extremely large Re).

(b) With rough walls, the dissipation again appears to go to a nonzero limit as $Re \to \infty$.

The paper of O. Cadot et al. Phys. Rev. E 56: 427 (1997) studies several flows, e.g. the "French Washing Machine" and the Couette-Taylor cell.

Their conclusion is that

(i) The dissipation in the boundary layer, where the production mechanism is Reynolds-number dependent, appears also to decrease slowly with the Reynolds number.

(ii) The dissipation in the bulk of the flow, away from the walls, is apparently independent of the Reynolds number Re.

Summary: This brief survey of key experiments supports the conclusion that turbulent energy dissipation rates become Re-independent at high Reynolds number. We shall re-examine the evidence more closely after developing more theory. A recent article

J. C. Vassilicos, "Dissipation in Turbulent Flows," Annu. Rev. Fluid Mech. 47: 95–114 (2015)

contains a rather comprehensive and useful review of data from laboratory experiments and numerical simulations (although the theoretical interpretations proposed in that paper differ a bit from those developed in this course).

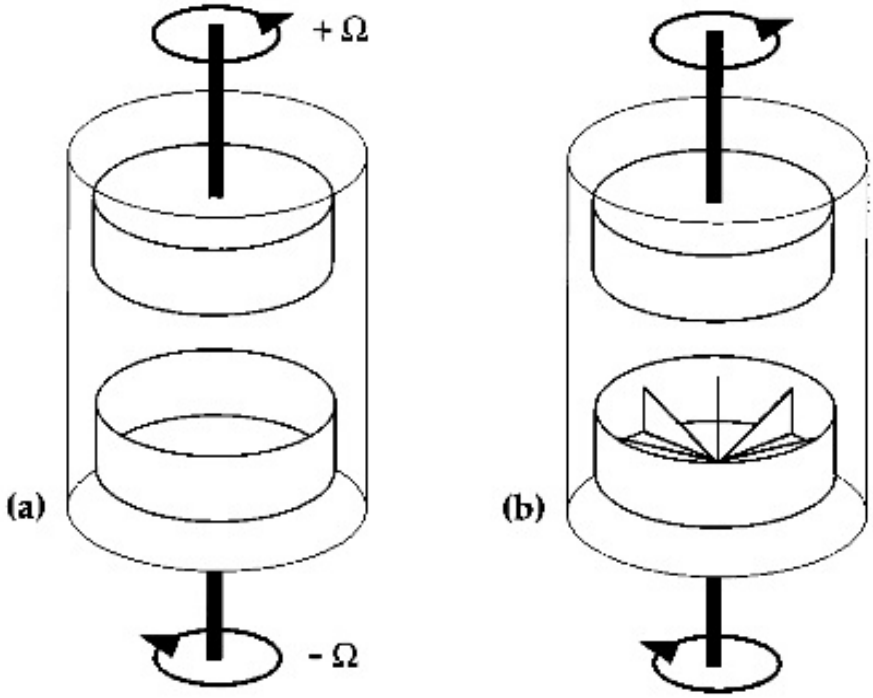

FIG. 1. Schemes of the two variants of experiment A. (a) Smooth stirrers: the two stirrers are disks with a cylindrical rim. (b) Rough or inertial stirrers: inside the rim, six blades are placed perpendicular to the disk surfaces and thus perpendicular to the rotation velocity.

Figure 12:

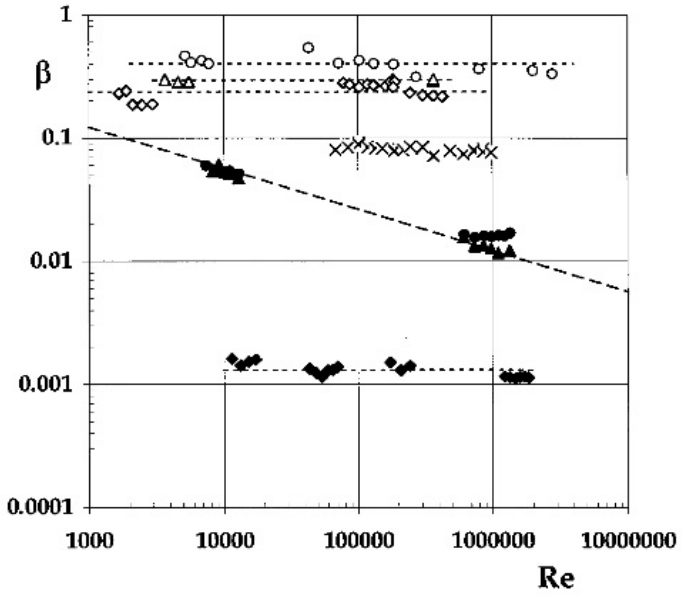

FIG. 2. Experiment A: Logarithmic plots of the nondimensional rate of energy injection β_I and dissipations β_D and β_B as a function of the Reynolds number for the three variants of the experiment. Black symbols: results obtained with smooth stirrers. Triangles (▲), rate of energy dissipation β_D; circles (●), rate of energy injection β_I; diamonds (♦), estimate of the rate of energy β_B dissipated in the bulk of the fluid as estimated from the pressure fluctuations. The dashed line shows a power law dependence proportional to $\mathrm{Re}^{-1/4}$. Open symbols: results obtained with the very rough (or inertial) stirrers. Triangles (△), rate of energy dissipation β_D; circles (○), rate of energy injection β_I; diamonds (◇), rate of energy dissipation β_B. Results are obtained with the stirrers having smaller platelets. × is the mean rate of the energy dissipation β_D.

Figure 13:

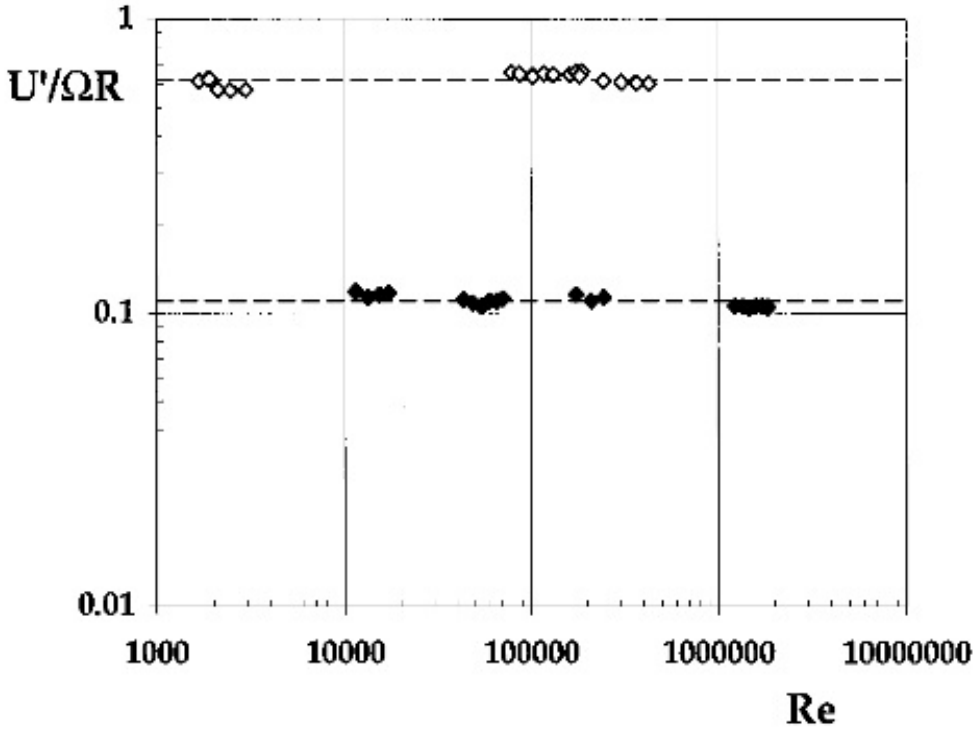

FIG. 3. Plot of the typical velocity U' in the bulk of the flow as deduced from the histograms of the pressure fluctuations [see Eq. (7)]. The black triangles (▲) are the data obtained with smooth stirrers, and the open ones (△) correspond to the data obtained with the rough ones.

Figure 14:

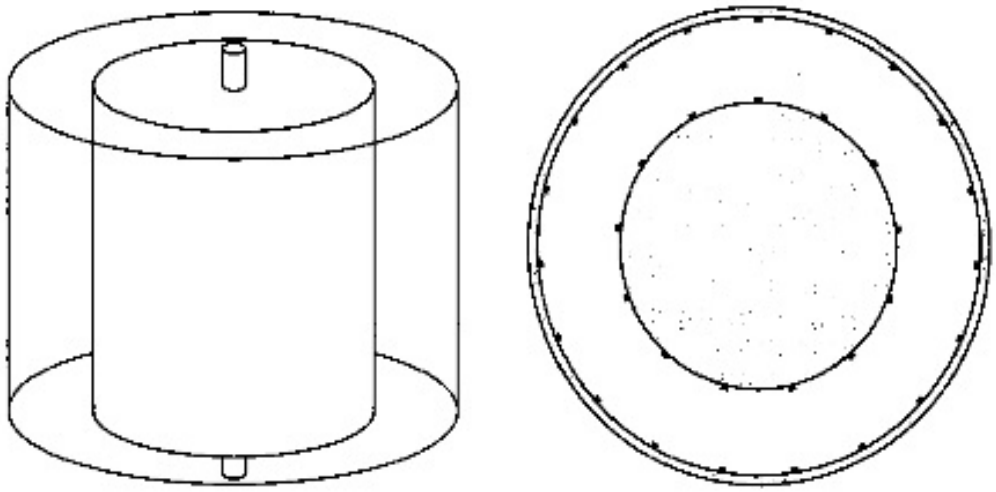

FIG. 4. Schemes of experiment B: (a) the Couette-Taylor cell with smooth surfaces and (b) the section of the system perpendicular to the axis of rotation and showing the ribs which make the walls rough.

Figure 15:

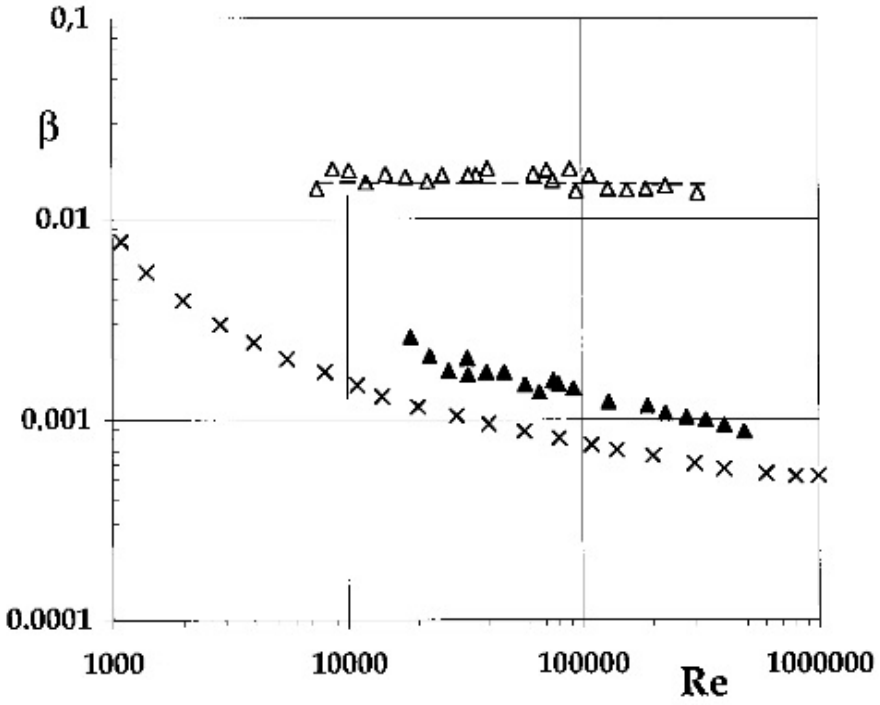

FIG. 5. Couette-Taylor experiments. Logarithmic plots of the nondimensional rates of energy dissipation β_D as a function of the Reynolds number. The black triangles (▲) are the results obtained with smooth cylinders, and the open ones (△) correspond to those obtained with the ribbed ones. The crosses (×) show for comparison the rates of energy injection β_D deduced from the data obtained with smooth cylinders by Lathrop, Finenberg, and Swinney [8].

Figure 16:

We have emphasized the enhanced dissipation in turbulent flow, but there are other phenomena as well. Another key property exhibited by turbulence is enhanced mixing/space-tranport of heat, momentum, kinetic energy, dyes, etc.

E.g. chemical engineers use turbulence to efficiently mix chemical reactants so that reaction rates are greatly accelerated. This is a practically beneficial aspect of turbulence.

Another example is turbulence efficiency at transporting air-borne chemicals and solutes in liquids. The reason that you can smell your significant other's perfume/cologne when they enter the room is because of small-scale turbulence in the air!

We focus in this course first on understanding enhanced turbulent energy dissipation. As a matter of fact, this turns out to be very closely related to the transport/mixing properties, which we discuss later. The enhanced spatial dispersion of particles by turbulence was pointed out by Lewis Fry Richardson already in (1926), who proposed that mean-square separation of particles grows super-diffusively as

$$\langle |\mathbf{x}_1(t) - \mathbf{x}_2(t)| \sim \varepsilon t^3.$$

This proposal has been well-confirmed by recent, highly resolved numerical simulations (but is still not conclusively seen in controlled laboratory experiments), e.g. R. Bitane et al. "Geometry and violent events in turbulent pair dispersion," J. Turbulence, 14: 2 (2013).

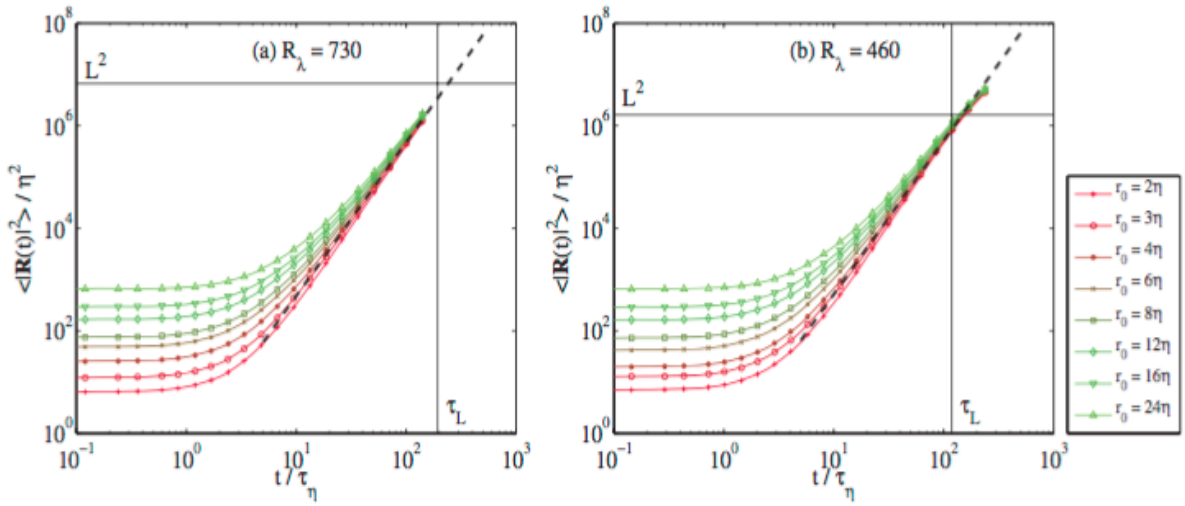

Figure 2. Time-evolution of the mean-squared distance for $R_\lambda = 730$ (a) and $R_\lambda = 460$ (b) for various initial separations r_0 as labeled. The horizontal and vertical solid lines represent the integral scale L and its associated turnover time τ_L, respectively. The dashed line corresponds to the explosive Richardson–Obukhov law (3) with $g = 0.52$.

Figure 17: From Bitane et al. (2013)

Another important aspect of turbulence is its unpredictability. This is a property difficult to measure in laboratory experiment, due to the lack of fine control in in-flow conditions, etc. However, it is found in numerical simulations that two flows with slightly different initial conditions $\mathbf{u}_1(\mathbf{x})$, $\mathbf{u}_2(\mathbf{x})$ have an error energy

$$E_\Delta(t) = \frac{1}{2}\int d^d x |\mathbf{u}_1(\mathbf{x},t) - \mathbf{u}_2(\mathbf{x},t)|^2$$

which grows as

$$E_\Delta(t) \sim G\varepsilon t$$

with $G \simeq 0.45$ (in 3D), roughly consistent with a prediction of Leith & Kraichnan (1972).

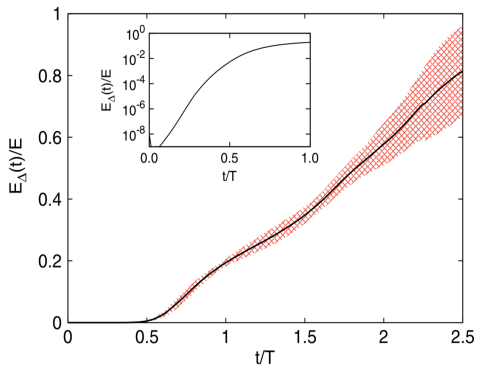

FIG. 1. Error energy $E_\Delta(t)$ growth for the simulation at $N = 1024$. The error energy is averaged over ten different realizations (black line). The fluctuations of the error energy within one standard deviation from the mean are represented by the shaded area. Inset: The initial exponential growth of the error.

Figure 18: From G. Boffetta and S. Musacchio, "Chaos and predictability of homogeneous-isotropic turbulence," PRL **119** 054102 (2017). See also A. Berera and R. D. J. G. Ho, "Chaotic properties of a turbulent isotropic fluid," **120** 024101 (2018).